

Free-GVC: Towards Training-Free Extreme Generative Video Compression with Temporal Coherence

Xiaoyue Ling, Chuqin Zhou, Chunyi Li, Yunuo Chen, Yuan Tian, Guo Lu, *Member, IEEE*,
Wenjun Zhang, *Fellow, IEEE*

Abstract—Building on recent advances in video generation, generative video compression has emerged as a new paradigm for achieving visually pleasing reconstructions. However, existing methods exhibit limited exploitation of temporal correlations, causing noticeable flicker and degraded temporal coherence at ultra-low bitrates. In this paper, we propose Free-GVC, a training-free generative video compression framework that reformulates video coding as latent trajectory compression guided by a video diffusion prior. Our method operates at the group-of-pictures (GOP) level, encoding video segments into a compact latent space and progressively compressing them along the diffusion trajectory. To ensure perceptually consistent reconstruction across GOPs, we introduce an Adaptive Quality Control module that dynamically constructs an online rate–perception surrogate model to predict the optimal diffusion step for each GOP. In addition, an Inter-GOP Alignment module establishes frame overlap and performs latent fusion between adjacent groups, thereby mitigating flicker and enhancing temporal coherence. Experiments show that Free-GVC achieves an average of 93.29% BD-Rate reduction in DISTS over the latest neural codec DCVC-RT, and a user study further confirms its superior perceptual quality and temporal coherence at ultra-low bitrates.

Index Terms—Video Compression, Generative Model, Ultra-Low Bitrate.

I. INTRODUCTION

Video compression plays a vital role in managing the growing volume of visual content across streaming, storage, and communication systems. Conventional approaches, from traditional standards [1]–[3] to recent neural codecs [4]–[6], primarily rely on transform coding to reduce spatial and temporal redundancy by mapping pixels into compact representations. While these distortion-oriented codecs excel at preserving fidelity under moderate compression, they often fail to maintain perceptual realism at low bitrates, producing blocking artifacts and over-smoothed textures. Perception-oriented methods [7]–[9] shift the optimization target from pixel-level distortion to perceptual similarity, improving visual quality through adversarial training and perceptual losses. However, they still suffer from blurring under extreme compression due to the lack of strong generative priors. These limitations motivate the exploration of generative methods that can synthesize missing details and restore perceptual fidelity.

Among generative approaches, diffusion models have recently emerged as a powerful paradigm for image and video

Xiaoyue Ling, Chuqin Zhou, Yunuo Chen, Guo Lu and Wenjun Zhang are with the Institute of Image Communication and Network Engineering, Shanghai Jiao Tong University, Shanghai 200240, China (e-mail: xiayou Ling, zhouchuqin, cyril-cheny, luguo2014, zhangwenjun@sjtu.edu.cn). (Corresponding author: Guo Lu.)

Chunyi Li and Yuan Tian are with the Shanghai AI Lab, Shanghai 200232, China (e-mail: lichunyi, tianyuan@pjlab.org.cn)

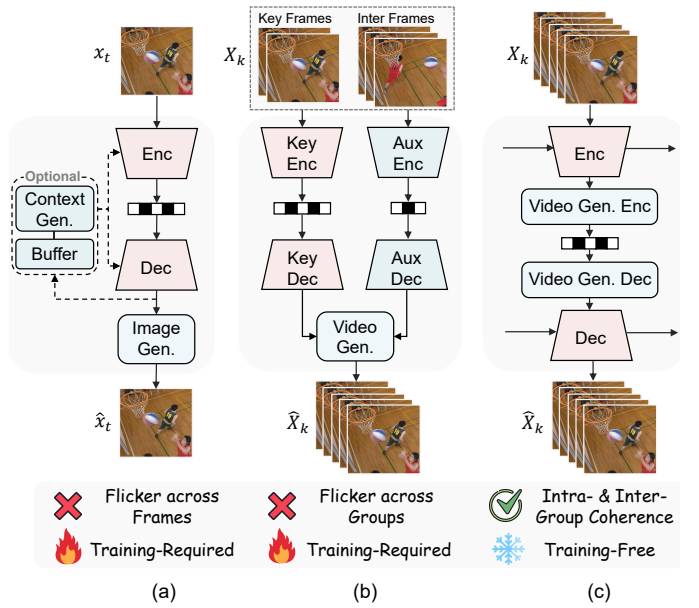


Fig. 1. Comparison of generative video compression paradigms. (a) Frame-wise generation introduces frame-level flicker and requires training. (b) Group-wise generation ignores correlations across adjacent groups, leading to temporal discontinuities, and also requires training. (c) Our training-free method fuses inter-group information to achieve temporally coherent compression.

synthesis [10]–[12], owing to their remarkable ability to model complex data distributions. This capability has inspired a new line of research in generative image compression [13]–[15], where pretrained diffusion priors are leveraged at the decoder to enhance highly compressed latent representations. By delegating fine-detail synthesis to these generative models, such methods achieve perceptually faithful reconstructions even at ultra-low bitrates.

Compared to images, videos introduce an additional temporal dimension, posing greater challenges for exploiting generative priors in compression, as illustrated in Fig. 1. A straightforward approach is to apply generative image codecs [17], [18] in a frame-by-frame manner. While this yields visually rich details within each frame, it ignores inter-frame dependencies, leading to temporal flicker and inconsistency. To improve temporal coherence, some works integrate frame-wise generation into neural video compression (NVC) frameworks [16], [19], where the encoder captures temporal redundancy and the decoder employs generative models for



Fig. 2. Qualitative comparison at ultra-low bitrates. The left part illustrates temporal coherence measured by tOF, while the right part compares perceptual quality evaluated by DISTs. Free-GVC achieves the best perceptual quality at the lowest bitrate while maintaining strong temporal consistency. Distortion-oriented codecs, including VVC [3], DCVC-RT [5], and DCVC-FM [4], preserve temporal coherence but suffer from perceptual degradation. In contrast, generative codecs such as GLC-Video [16] produce rich textures but exhibit misalignment with the ground truth and adjacent frames. ↓ indicates lower values are better.

reconstruction. However, the inherent stochasticity of generative models still causes variations across frames, leaving the flicker issue unresolved. Another line of work operates at the group-of-pictures (GOP) level [20], [21], improving compression efficiency by transmitting only keyframes with minimal auxiliary information, such as text prompts or optical flow, and generating the remaining frames at the decoder using video diffusion models. While this approach reduces bitrate, it often compromises the fidelity of non-keyframes. Moreover, by processing each GOP independently, these methods largely ignore correlations between neighboring segments, leading to temporal discontinuities and flicker across GOPs.

In summary, while generative approaches improve perceptual realism over conventional distortion- or perception-oriented codecs, they still struggle to maintain temporal coherence at ultra-low bitrates, as illustrated in Fig. 2. This limitation is further exacerbated in dynamic scenes, where variations in content and motion induce inconsistent generative behavior over time. More fundamentally, diffusion-based generative compression with a fixed diffusion step is inherently ill-posed for video, as the stochastic generative process synthesizes different levels of detail across contents, preventing a consistent rate–perception trade-off and resulting in temporal quality fluctuations. Moreover, most existing methods [16], [17], [19] require extensive retraining or fine-tuning to adapt pretrained generative models for compression.

To address these issues, we propose Free-GVC, a training-free generative video compression framework that reformulates compression as progressive coding of noisy latent representations in the diffusion space, with noise level corresponding to bitrate. Specifically, the input video is divided into GOPs and projected into a compact latent space, where each group is iteratively refined along the diffusion trajectory from pure Gaussian noise to a clean reconstruction under the guidance of a pretrained video diffusion prior. This design enables compression while preserving intra-GOP temporal coherence.

To ensure perceptually consistent reconstruction, we introduce an Adaptive Quality Control module that dynamically constructs an online rate–perception surrogate model during encoding to predict the appropriate diffusion step for each GOP, maintaining stable perceptual quality across diverse content. Furthermore, an Inter-GOP Alignment mechanism enhances temporal continuity by establishing frame overlap during encoding and fusing shared latent features during decoding, effectively mitigating flicker and boundary misalignment.

Our main contributions are summarized as follows:

- We propose Free-GVC, a training-free generative video compression framework that recasts video coding as diffusion-guided latent trajectory compression, enabling perceptually faithful reconstruction at ultra-low bitrates.
- We design an Adaptive Quality Control module and an Inter-GOP Alignment mechanism, which jointly enhance perceptual stability and temporal coherence across GOPs.
- Extensive experiments show that Free-GVC achieves an average of 93.29% BD-Rate savings in DISTs across HEVC Class B~E, UVG, and MCL-JCV datasets compared with the latest neural codec DCVC-RT, while a user study further confirms its perceptual and temporal advantages even at half the bitrate of DCVC-RT.

II. RELATED WORKS

A. Neural Video Compression

In recent years, NVC has attracted increasing attention [6], [22]–[28]. DVC [28] introduces the first end-to-end framework that jointly optimizes all components of the conventional hybrid coding framework. The DCVC series [4], [5], [29], [30] replaces explicit residual coding with conditional mechanisms, while subsequent variants further enhance context modeling. Lu *et al.* [31], [32] adopt hierarchical variational autoencoders (VAEs) to probabilistically model multi-scale latent features. Despite these advances, distortion-oriented approaches that optimize pixel-level fidelity metrics, such as MSE or PSNR,

often produce overly smoothed reconstructions at low bitrates, degrading perceptual realism. To address this, several studies adopt perception-oriented training objectives. For example, DVCP [33] and NVCGAN [8] employ LPIPS [34] and adversarial losses [35] to improve perceptual quality. PLVC [9] employs a recurrent conditional discriminator, and HVFVC [7] proposes a confidence-based feature reconstruction strategy. While these methods produce more visually appealing results, the lack of strong generative priors limits their ability to preserve perceptual fidelity at ultra-low bitrates.

B. Generative Video Compression

A straightforward way to exploit generative priors for video compression is to process videos frame by frame using generative image codecs such as DiffC [18] and StableCodec [17]. However, since these models are optimized for images, they overlook inter-frame redundancy and temporal dependencies, leading to suboptimal compression efficiency and noticeable temporal inconsistency. To better leverage generative priors and remove temporal redundancy for video compression, a variety of dedicated generative video compression approaches have been proposed. One representative direction involves tokenizer-based methods. For instance, GLC-Video [16] leverages VQGAN [36] to extract perceptually meaningful latent features for efficient compression. Another major line of research focuses on diffusion-based approaches. DiffVC series [19], [37] extend NVC architectures by integrating a VAE for feature extraction and employing an image diffusion model at the decoder to recover fine details. Other studies [20], [21] improve efficiency by transmitting only key frames and minimal side information, with a video diffusion model synthesizing the remaining frames at the decoder. By leveraging powerful generative priors for content reconstruction, generative compression demonstrates strong potential at ultra-low bitrates, though maintaining temporal coherence and perceptual quality remains a key challenge. Distinct from prior works requiring codec redesign or model retraining, we propose a training-free framework that directly exploits pretrained video diffusion priors for high-quality generative compression with temporally consistent reconstruction.

C. Quality Control Mechanism

Quality control has long been a fundamental challenge in video compression. Traditional codecs rely on a well-established rate-distortion optimization framework [38]–[40], where quantization parameters are adaptively tuned to balance bitrate and reconstruction fidelity. Similar principles have been extended to NVC [41]–[43]. DCVC-FM [4] introduces a quantization scaler and buffer-based control mechanism to regulate frame rates. Zhang *et al.* [44] further redistribute bits across frames to enhance overall coding efficiency. Gu *et al.* [45] and Feng *et al.* [46] introduce modules that predict rate-distortion curves and optimize bitrate allocation accordingly.

These approaches assume a deterministic mapping between coding parameters and reconstruction quality, an assumption that no longer holds in generative compression. The stochastic

generation process produces content-dependent detail variations, leading to inconsistent perceptual quality. In this work, we explore an adaptive quality control strategy that builds an online rate–perception surrogate during encoding to select appropriate diffusion steps for each GOP, ensuring stable perceptual quality across diverse video content despite the stochastic nature of diffusion-based reconstruction.

III. PRELIMINARIES

Our compression framework builds upon reverse channel coding (RCC), a principled approach that leverages diffusion models for progressive lossy compression. This section briefly reviews the theoretical foundation and practical implementation of RCC.

A. Diffusion Models as Lossy Compression

DDPM [47] can be interpreted as a form of progressive lossy source coding that attempts to transmit a clean data sample \mathbf{x}_0 , drawn from the data distribution $q(\mathbf{x}_0)$, through the forward and reverse diffusion processes. The framework relies on minimal random coding [48], [49], which enables transmitting a random variable $\mathbf{x} \sim q(\mathbf{x})$ using approximately $D_{KL}(q(\mathbf{x}) \parallel p(\mathbf{x}))$ bits on average, where $p(\mathbf{x})$ is a known prior distribution for both the sender and the receiver.

When this principle is applied to $\mathbf{x}_0 \sim q(\mathbf{x}_0)$, the diffusion trajectory induces a progressive lossy source coding procedure. Specifically, a sequence of latent variables $\{\mathbf{x}_t\}_{t=0}^T$ is constructed, where \mathbf{x}_T represents the fully noised latent at the final diffusion step T and \mathbf{x}_t represents the latent at intermediate timestep t . These variables are sequentially communicated from \mathbf{x}_T to \mathbf{x}_0 . At each step, the forward posterior $q(\mathbf{x}_t \mid \mathbf{x}_{t+1}, \mathbf{x}_0)$ is encoded using the learned reverse distribution $p_\theta(\mathbf{x}_t \mid \mathbf{x}_{t+1})$, where θ denotes the model parameters.

At any intermediate timestep t , the receiver has full access to the partial latent \mathbf{x}_t and can directly estimate the original signal \mathbf{x}_0 via

$$\mathbf{x}_0 \approx \hat{\mathbf{x}}_0 = (\mathbf{x}_t - \sqrt{1 - \bar{\alpha}_t} \epsilon_\theta(\mathbf{x}_t, t)) / \sqrt{\bar{\alpha}_t}, \quad (1)$$

where $\epsilon_\theta(\mathbf{x}_t, t)$ denotes the noise prediction network, $\alpha_t := 1 - \beta_t$ is the signal preservation factor at timestep t , $\bar{\alpha}_t := \prod_{s=1}^t \alpha_s$ is the cumulative product controlling the overall noise level, and $\beta_t \in (0, 1)$ specifies a monotonically increasing variance schedule. Alternatively, rather than directly estimating \mathbf{x}_0 from \mathbf{x}_t , the receiver may stochastically reconstruct the entire reverse trajectory $\mathbf{x}_t, \mathbf{x}_{t-1}, \dots, \mathbf{x}_0$ to achieve higher perceptual quality through the full generative process.

B. Practical Implementation

This lossy compression interpretation is practically instantiated through RCC [15], [18], [50], which employs the Poisson Functional Representation (PFR) algorithm [51] to transmit samples from a target distribution q using only a source distribution p , as shown in Algorithms 1 and 2. PFR generates candidate samples from p using different random seeds n via a shared pseudorandom generator simulate, and selects the seed n^* that minimizes the likelihood-ratio score.



Fig. 4. Progressive compression process of frame 24 from the videoSRC25 sequence in the MCL-JCV dataset.

the diffusion trajectory from timestep T to t^* , yielding the noisy latent \mathbf{z}_{t^*} , which is then compressed into a bitstream using RCC [50]. At the decoder side, the transmitted latent \mathbf{z}_{t^*} is denoised to obtain the clean latent $\hat{\mathbf{y}}_k$. The Inter-GOP Alignment mechanism then fuses latents in the overlapping regions, effectively suppressing flicker and boundary artifacts to ensure smooth transitions across GOPs. Finally, the fused latent $\hat{\mathbf{y}}_k$ is passed through the VAE decoder \mathcal{D} to produce perceptually faithful reconstructions $\hat{\mathbf{X}}_k$.

B. Diffusion Trajectory Compression

Building on the RCC framework introduced in Section III, we now describe how GOP \mathbf{X}_k is compressed by progressively coding along the diffusion trajectory. The compression process begins from a random Gaussian sample $\mathbf{z}_T \sim \mathcal{N}(0, I)$ and proceeds toward the target latent \mathbf{y}_k , terminating at an adaptive timestep t^* determined by the quality control module.

At each denoising step t from T to t^* , the encoder leverages the video diffusion prior p_θ , which operates on the GOP through its spatiotemporal attention and 3D causal convolutional architecture to implicitly preserve temporal coherence. The PFR algorithm (Algorithms 1 and 2) searches for optimal random seeds that align the predicted distribution $p_\theta(\mathbf{z}_t | \mathbf{z}_{t+1})$ with the true posterior $q(\mathbf{z}_t | \mathbf{z}_{t+1}, \mathbf{y}_k)$. Specifically, each candidate seed n generates a latent \mathbf{z}_n sampled from $p_\theta(\mathbf{z}_t | \mathbf{z}_{t+1})$ via the shared pseudorandom generator, and the encoder selects the seed n whose \mathbf{z}_n minimizes the divergence from the target posterior. Once the optimal seeds from step T to t^* are determined, they are entropy-coded together. The resulting bitrate for GOP k is given by:

$$R_k = \frac{\sum_{t=t^*}^{T-1} D_{\text{KL}}(q(\mathbf{z}_t | \mathbf{z}_{t+1}, \mathbf{y}_k) \| p_\theta(\mathbf{z}_t | \mathbf{z}_{t+1}))}{l \times H \times W}, \quad (7)$$

where l denotes the GOP length, and H and W are the spatial dimensions of each frame. This approach transmits only compact random seeds rather than high-dimensional latents, significantly reducing bandwidth requirements.

At the decoder side, the transmitted seeds regenerate \mathbf{z}_{t^*} using the shared diffusion prior. The partially denoised latent is then progressively refined through the remaining reverse diffusion steps $t^* \rightarrow 0$ to obtain the clean latent $\hat{\mathbf{y}}_k$. Finally, the VAE decoder reconstructs perceptually faithful frames.

An important property of this framework is its ability to provide continuous quality scaling. By adjusting the termination timestep t^* , the compressed bitrate can be naturally controlled. As illustrated in Fig. 4, at the lowest bitrate, the reconstructed frame successfully preserves the overall structure and global semantics of the scene, although fine details and subtle textures are noticeably degraded. As the bitrate increases by transmitting more diffusion steps, these discrepancies gradually diminish: finer textures, object boundaries, and high-frequency details are progressively restored, and the reconstructed frame becomes nearly indistinguishable from the original. This progressive behavior highlights the inherent capability of our diffusion-based framework to provide flexible bitrate control without retraining or additional overhead.

We also provide some theoretical insights to demonstrate the advantages of applying RCC with a joint spatiotemporal prior over frame-wise generative compression approaches. To understand how temporal coherence is preserved in our framework, consider the autoregressive factorization of the diffusion prior across the temporal dimension, which arises naturally from the causal design of video VAE encoders [52], [53]:

$$p_\theta(\mathbf{z}_t | \mathbf{z}_{t+1}) = \prod_{i=1}^{l'} p_\theta\left(\mathbf{z}_t^{(i)} \mid \mathbf{z}_t^{(<i)}, \mathbf{z}_{t+1}\right), \quad (8)$$

where $l' = l/s$ denotes the temporal dimension of the latent representation with s being the VAE temporal downsampling factor, $\mathbf{z}_t^{(<i)} = \{z_t^{(1)}, \dots, z_t^{(i-1)}\}$ denotes the already-decoded frames at the current timestep t , and \mathbf{z}_{t+1} represents the noisy state from the previous diffusion step. This conditioning structure means that when sampling frame i at timestep t , the model has access to both (1) the noisier state \mathbf{z}_{t+1} from the previous diffusion step, and (2) the previous latent frames $\mathbf{z}_t^{(<i)}$ that have already been generated at the current step. This dual conditioning enables the model to maintain temporal consistency while progressively refining details.

Similarly, the true posterior conditioned on the clean latent \mathbf{y}_k can be written as:

$$q(\mathbf{z}_t | \mathbf{z}_{t+1}, \mathbf{y}_k) = \prod_{i=1}^{l'} q\left(z_t^{(i)} \mid \mathbf{z}_t^{(<i)}, \mathbf{z}_{t+1}, \mathbf{y}_k^{(\leq i)}\right), \quad (9)$$

where the conditioning on $\mathbf{y}_k = \{y_k^{(1)}, \dots, y_k^{(l')}\}$ provides the ground-truth temporal context.

Algorithm 3 Adaptive Quality Control

Input: Latent \mathbf{y}_k , target quality P_{tar} , previous set Φ_{k-1}
Output: Encoded latent \mathbf{z}_{t^*} , updated set Φ_k

```

1: if  $\Phi_{k-1} = \emptyset$  then
   // Sparse Timestep Sampling
2:   Initialize  $\mathbf{z}_T \sim \mathcal{N}(0, I)$ 
3:   Select sampling set  $\mathcal{S} \subset \{1, \dots, T\}$  with  $|\mathcal{S}| = M$ 
4:   for  $t = T - 1$  to 0 do
5:     if  $|\Phi_k| = M$  then break
6:     Encode  $\mathbf{z}_t \sim q(\mathbf{z}_t | \mathbf{z}_{t+1}, \mathbf{y}_k)$  using  $p_\theta(\mathbf{z}_t | \mathbf{z}_{t+1})$ 
7:     if  $t \in \mathcal{S}$  then
8:       Compute  $(R_t, P_t)$  from  $\mathbf{z}_t$ 
9:        $\Phi_k \leftarrow \Phi_k \cup \{(R_t, P_t)\}$ 
10:    end if
11:   end for
12: else
   // History Information Reuse
13:    $\Phi_k \leftarrow \text{align}(\Phi_{k-1})$ 
14: end if
   // Iterative Refinement
15: while  $|P_{t^*} - P_{tar}| > \varepsilon$  do
   // Online Surrogate Fitting
16:    $\alpha_k, \beta_k \leftarrow \arg \min_{\alpha, \beta} \sum_{(R_i, P_i) \in \Phi_k} [P_i - (\alpha \cdot R_i^\beta)]^2$ 
17:    $R^* \leftarrow (P_{tar}/\alpha_k)^{\frac{1}{\beta_k}}$ 
18:    $t^* \leftarrow \arg \min_t |R_t - R^*|$ 
19:   Encode  $\mathbf{z}_{t^*} \sim q(\mathbf{z}_{t^*} | \mathbf{z}_{t^*+1}, \mathbf{y}_k)$  using  $p_\theta(\mathbf{z}_{t^*} | \mathbf{z}_{t^*+1})$ 
20:   Compute  $(R_{t^*}, P_{t^*})$  from  $\mathbf{z}_{t^*}$ 
21:    $\Phi_k \leftarrow \Phi_k \cup \{(R_{t^*}, P_{t^*})\}$ 
22:    $\Phi_k \leftarrow \Phi_k \setminus \{\arg \max_{(R_i, P_i) \in \Phi_k} |P_i - P_{tar}|\}$ 
23: end while
24: return  $\mathbf{z}_{t^*}, \Phi_k$ 

```

In contrast, frame-wise generative compression applies an image diffusion model independently to each frame in the latent space. In such methods, the prior factorizes as:

$$p_\theta^{\text{fw}}(\mathbf{z}_t | \mathbf{z}_{t+1}) = \prod_{i=1}^{l'} p_\theta^{(i)} \left(z_t^{(i)} \mid z_{t+1}^{(i)} \right), \quad (10)$$

where each frame i is processed independently without access to temporal context $\mathbf{z}_t^{(<i)}$ or causal frames in \mathbf{y}_k . The corresponding posterior similarly factorizes:

$$q^{\text{fw}}(\mathbf{z}_t | \mathbf{z}_{t+1}, \mathbf{y}_k) = \prod_{i=1}^{l'} q \left(z_t^{(i)} \mid z_{t+1}^{(i)}, y_k^{(i)} \right). \quad (11)$$

The coding cost for frame-wise compression at step t is:

$$L_t^{\text{fw}} = \sum_{i=1}^{l'} D_{\text{KL}} \left(q(z_t^{(i)} | z_{t+1}^{(i)}, y_k^{(i)}) \parallel p_\theta^{(i)}(z_t^{(i)} | z_{t+1}^{(i)}) \right), \quad (12)$$

whereas for our joint model:

$$L_t^{\text{joint}} = D_{\text{KL}} (q(\mathbf{z}_t | \mathbf{z}_{t+1}, \mathbf{y}_k) \parallel p_\theta(\mathbf{z}_t | \mathbf{z}_{t+1})). \quad (13)$$

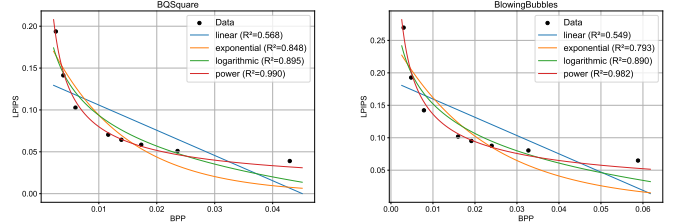


Fig. 5. Fitting performance of different models for the relationship between bitrate and perception across different sequences.

Using the chain rule of KL divergence, we can show that:

$$L_t^{\text{fw}} - L_t^{\text{joint}} = \sum_{i=1}^{l'} I_q \left(z_t^{(i)}; \mathbf{z}_t^{(<i)}, \{z_{t+1}^{(j)}\}_{j \neq i}, \{y_k^{(j)}\}_{j < i} \mid z_{t+1}^{(i)}, y_k^{(i)} \right) \geq 0, \quad (14)$$

where $I_q(\cdot; \cdot)$ denotes the conditional mutual information. This result reveals that frame-wise compression incurs an additional coding cost equal to the mutual information between each frame and its temporal context, which could otherwise be exploited by a joint model to reduce the bitrate. For a detailed proof and further discussion of this result, we refer the reader to the supplementary material.

When RCC is applied over $T - t^*$ diffusion steps, this gap accumulates:

$$\sum_{t=t^*}^{T-1} (L_t^{\text{fw}} - L_t^{\text{joint}}) \geq 0, \quad (15)$$

resulting in either higher bitrate or degraded perceptual quality for frame-wise methods at the same target rate.

C. Adaptive Quality Control

In diffusion-based video compression, bitrate control presents a fundamentally different challenge compared to conventional codecs. Due to content variation across GOPs and the inherent randomness of diffusion sampling, a fixed diffusion step may yield substantially different bitrates and perceptual quality for different video segments. This stochastic behavior can cause noticeable quality fluctuations across GOPs, which is particularly detrimental to temporal coherence.

To address this issue, we formulate quality control in diffusion-based compression as an online inverse rate-perception mapping problem. Given a target perceptual quality P_{tar} , the goal is to determine an appropriate diffusion timestep such that the expected coding rate and reconstruction quality match the target with minimal deviation. As detailed in Section IV-B, our progressive encoding paradigm naturally supports rollback to any previous timestep without re-encoding, enabling efficient quality control with minimal overhead. The complete procedure is outlined in Algorithm 3.

1) *Sparse Timestep Sampling*: During encoding, M candidate timesteps are uniformly sampled from the diffusion schedule of T steps, forming the set S . For each sampled

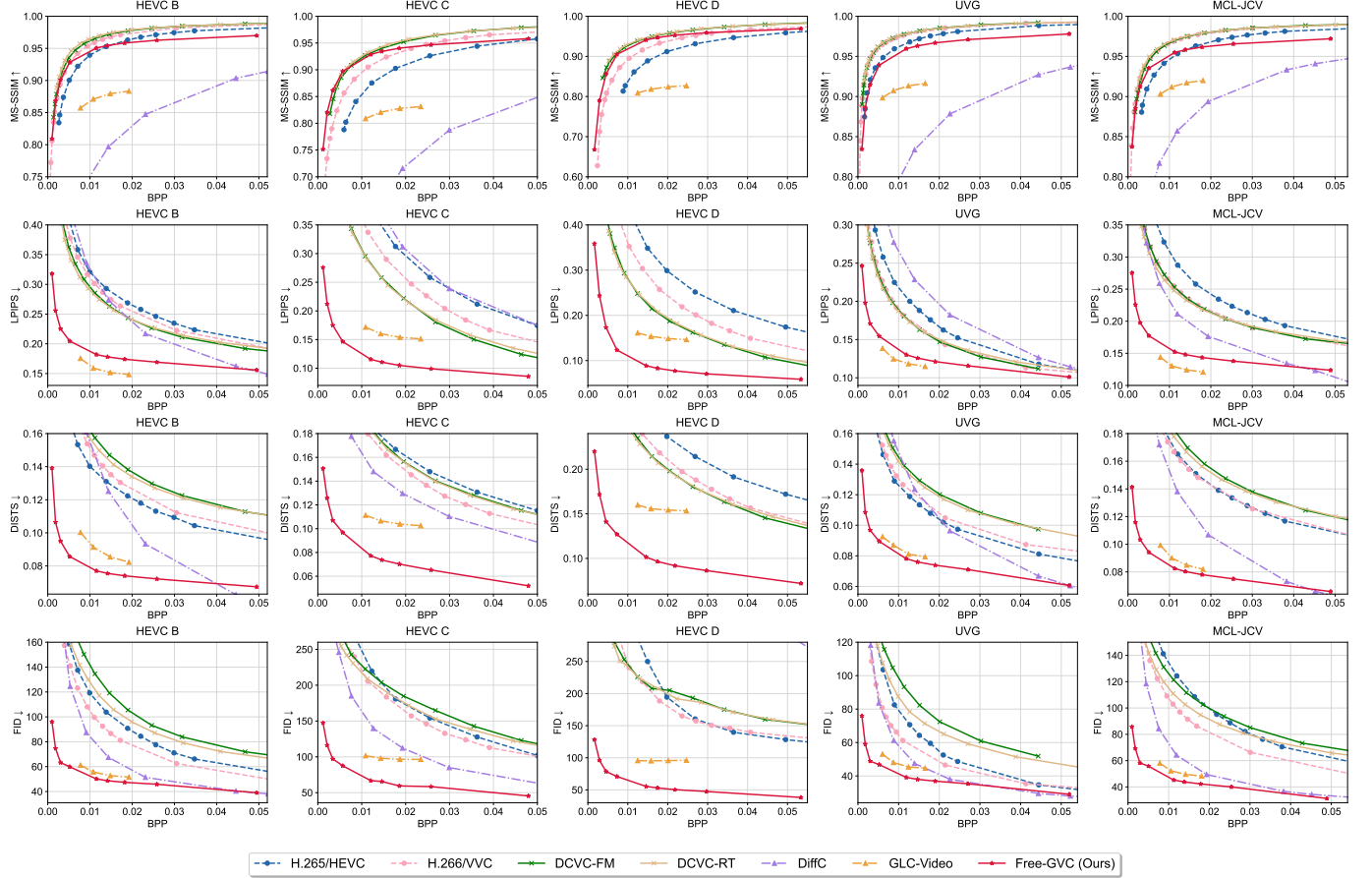


Fig. 6. Rate–Metric curves on HEVC B~D, UVG, and MCL-JCV datasets measured by MS-SSIM, LPIPS, DISTs, and FID.

timestep, the current state is decoded, with the resulting bitrate R_t and perceptual quality P_t calculated and recorded in Φ_k . This sparse sampling process provides a set of anchor points that characterize the local rate–perception behavior of the current GOP, enabling efficient construction of a surrogate model without exhaustively traversing the entire diffusion trajectory.

2) *Online Surrogate Fitting*: Given the sampled rate–perception pairs $\Phi_k = \{(R_i, P_i)\}_{i=1}^M$, we construct a lightweight surrogate model to approximate the local relationship between bitrate R and perceptual quality P for the current GOP. Rather than assuming a global analytical form, the surrogate is fitted online and updated dynamically to adapt to content variations.

We adopt a power-law formulation $P = \alpha \cdot R^\beta$ as the surrogate function due to its strong empirical fitting accuracy and its consistency with classical rate–distortion behavior observed in both traditional and learned codecs [39], [40]. As shown in Fig. 5, the power model achieves consistently higher goodness-of-fit (R^2) across diverse video content compared to linear, logarithmic, and exponential alternatives. Importantly, the surrogate model serves not as a precise analytical description of the underlying rate–perception mechanism, but as an efficient inverse mapping tool that enables reliable prediction of diffusion step for bitrate targeting.

The parameters α_k and β_k are estimated by solving the

following regression problem:

$$\min_{\alpha, \beta} \sum_{(R_i, P_i) \in \Phi_k} [P_i - (\alpha \cdot R_i^\beta)]^2, \quad (16)$$

where α and β control the scale and nonlinearity of the fitted rate–perception curve, respectively. The corresponding target bitrate is predicted as $R^* = (P_{tar}/\alpha_k)^{\frac{1}{\beta_k}}$.

3) *Iterative Refinement*: Once the target bitrate R^* is predicted, the optimal timestep t^* is determined by $t^* = \arg \min_i |R_i - R^*|$, where R_i denotes the bitrate corresponding to timestep i . The selected state is then decoded and evaluated, yielding the pair (R_{t^*}, P_{t^*}) , which is added to the current observation set Φ_k .

This iterative refinement process can be interpreted as a feedback control mechanism, where the deviation between the achieved and target perceptual quality is progressively minimized. If the predicted perceptual quality P_{t^*} deviates from the target P_{tar} by more than a threshold ε , the model fitting and prediction steps are repeated with the updated Φ_k . By continuously updating the surrogate model with newly observed samples, the control loop converges rapidly to a stable diffusion step that satisfies the target quality constraint with minimal overhead. To maintain a stable fitting model, the sample farthest from P_{tar} is removed before refitting, ensuring that the most representative points guide subsequent predictions. Through empirical evaluation, we set $\varepsilon = 0.005$,

TABLE I. BD-Rate (%) and BD-Metric comparison on HEVC B~E, UVG, and MCL-JCV datasets. \downarrow and \uparrow denote that lower or higher BD-Metric values are better, respectively, depending on the metric. Negative BD-Rate values denote bitrate savings. Best and second-best results are highlighted in **red** and **blue**. “N/A” indicates that BD-rate cannot be computed due to insufficient overlap between the rate–metric curves.

Dataset	Metric	Traditional Codec		Neural Codec		Generative Codec	
		HEVC [2]	VVC [3]	DCVC-FM [4]	DCVC-RT [5]	GLC-Video [16]	Free-GVC (Ours)
HEVC B	MS-SSIM \uparrow	102.24 / -0.0211	32.74 / -0.0062	8.24 / -0.0035	0.00 / 0.0000	N/A / -0.0963	50.47 / -0.0166
	LPIPS \downarrow	50.85 / 0.0416	23.76 / 0.0196	5.18 / 0.0046	0.00 / 0.0000	-91.74 / -0.1167	-87.19 / -0.1107
	DISTS \downarrow	-31.68 / -0.0149	-14.67 / -0.0068	12.02 / 0.0050	0.00 / 0.0000	-89.81 / -0.0603	-95.32 / -0.0818
	FID \downarrow	-9.47 / -5.134	-33.59 / -19.326	28.80 / 12.533	0.00 / 0.0000	-89.22 / -62.8868	-95.37 / -77.8182
HEVC C	MS-SSIM \uparrow	157.87 / -0.0488	61.53 / -0.0227	5.50 / -0.0025	0.00 / 0.0000	N/A / -0.1245	31.90 / -0.0027
	LPIPS \downarrow	85.16 / 0.0841	36.66 / 0.0441	-0.10 / -0.0001	0.00 / 0.0000	-57.07 / -0.0856	-89.49 / -0.1567
	DISTS \downarrow	12.44 / 0.0061	-11.68 / -0.0088	2.63 / 0.0015	0.00 / 0.0000	-73.74 / -0.0610	-95.26 / -0.1012
	FID \downarrow	13.64 / 7.342	-6.24 / -4.339	14.85 / 9.025	0.00 / 0.0000	N/A / -88.9025	-95.69 / -130.8080
HEVC D	MS-SSIM \uparrow	161.48 / -0.0444	69.74 / -0.0239	3.30 / -0.0016	0.00 / 0.0000	N/A / -0.1339	44.82 / -0.0061
	LPIPS \downarrow	120.77 / 0.1027	49.26 / 0.0581	-0.71 / -0.0008	0.00 / 0.0000	-43.93 / -0.0555	-78.64 / -0.1334
	DISTS \downarrow	69.11 / 0.0357	15.73 / 0.0101	1.18 / 0.0009	0.00 / 0.0000	-66.58 / -0.0534	-89.25 / -0.1143
	FID \downarrow	11.55 / 1.9473	-14.56 / -8.6531	4.30 / 2.3789	0.00 / 0.0000	N/A / -110.9691	-97.38 / -161.3781
HEVC E	MS-SSIM \uparrow	91.26 / -0.0107	59.17 / -0.0059	-9.63 / 0.0006	0.00 / 0.0000	N/A / -0.0541	357.43 / -0.0133
	LPIPS \downarrow	30.49 / 0.0206	32.96 / 0.0189	-11.41 / -0.0059	0.00 / 0.0000	-80.80 / -0.0444	-89.55 / -0.0689
	DISTS \downarrow	-9.44 / -0.0052	-12.59 / -0.0054	-4.98 / -0.0022	0.00 / 0.0000	-54.36 / -0.0201	-89.46 / -0.0505
	FID \downarrow	38.93 / 17.9680	23.93 / 10.6847	2.64 / 1.1222	0.00 / 0.0000	-49.11 / -12.3345	-81.94 / -35.0579
UVG	MS-SSIM \uparrow	92.15 / -0.0175	7.55 / -0.0018	2.34 / -0.0009	0.00 / 0.0000	N/A / -0.0667	158.26 / -0.0245
	LPIPS \downarrow	57.14 / 0.0378	7.43 / 0.0060	1.02 / 0.0009	0.00 / 0.0000	-74.69 / -0.0634	-72.62 / -0.0615
	DISTS \downarrow	-26.55 / -0.0141	-24.36 / -0.0120	6.25 / 0.0029	0.00 / 0.0000	-88.74 / -0.0573	-93.66 / -0.0708
	FID \downarrow	-7.26 / -2.371	-42.51 / -21.498	26.22 / 9.348	0.00 / 0.0000	-79.02 / -40.6620	-93.51 / -56.1275
MCL-JCV	MS-SSIM \uparrow	105.05 / -0.0218	5.78 / -0.0018	8.25 / -0.0027	0.00 / 0.0000	N/A / -0.0583	63.72 / -0.0156
	LPIPS \downarrow	85.07 / 0.0538	10.49 / 0.0080	10.49 / 0.0076	0.00 / 0.0000	-91.91 / -0.1148	-88.28 / -0.1082
	DISTS \downarrow	-16.27 / -0.0088	-24.88 / -0.0137	12.24 / 0.0066	0.00 / 0.0000	-93.51 / -0.0863	-96.81 / -0.1026
	FID \downarrow	47.96 / 17.953	-15.20 / -6.948	30.70 / 10.323	0.00 / 0.0000	-92.10 / -57.2647	-96.35 / -70.0796

which achieves stable convergence with moderate iteration complexity while maintaining consistent perceptual control across diverse content.

4) *History Information Reuse*: To accelerate convergence and reduce redundant sampling, we exploit rate–perception similarity between consecutive GOPs. Instead of directly reusing the historical set Φ_{k-1} , an alignment point is first obtained by sampling a timestep t in the current GOP and measuring its (R_t, P_t) state. This alignment point scales and shifts Φ_{k-1} to match current GOP characteristics. The adjusted historical points are then combined with new samples to fit the updated model for GOP k . This history reuse strategy enables the control mechanism to exploit temporal consistency across neighboring GOPs, significantly reducing sampling overhead while preserving robustness to content changes.

D. Inter-GOP Alignment

Processing each GOP independently often causes visible discontinuities at GOP boundaries, especially in dynamic video scenes. To alleviate this, we design an Inter-GOP Alignment mechanism operating jointly across the encoding and decoding stages. It consists of two complementary parts: Frame Overlap at the encoder and Latent Fusion at the decoder.

1) *Frame Overlap*: During encoding, adjacent GOPs share m overlapping frames to maintain temporal continuity across boundaries. Specifically, for two consecutive GOPs \mathbf{X}_{k-1} and \mathbf{X}_k , the last m frames of \mathbf{X}_{k-1} are reused as the

first m frames of \mathbf{X}_k . Each GOP is then encoded into the latent space by the video VAE encoder, which downsamples the temporal dimension by a factor of s . Consequently, the overlapping region in the latent domain can be denoted as $\{\hat{y}_{k-1}^{(l'-i)}, \hat{y}_k^{(i)}\}_{i=1}^{m'}$, where $l' = l/s$ and $m' = m/s$.

2) *Latent Fusion*: At the decoding stage, overlapping latents are blended in the latent space to ensure smooth transitions at GOP boundaries. For each overlapping index $i \in \{1, \dots, m'\}$, we apply a weighted combination:

$$\tilde{y}_k^{(i)} = \gamma(i)\hat{y}_k^{(i)} + (1 - \gamma(i))\hat{y}_{k-1}^{(l'-i)}, \quad (17)$$

where $\gamma(i) \in [0, 1]$ is the fusion weight function that gradually shifts the contribution from the previous GOP to the current one. The fused latent \tilde{y}_k is then decoded to reconstruct $\hat{\mathbf{X}}_k = \mathcal{D}(\tilde{y}_k)$, thereby effectively suppressing boundary artifacts and maintaining temporal coherence across GOPs.

Since overlapping frames are redundantly encoded, this strategy introduces a slight bitrate overhead. For a video with K GOPs, each containing l frames, $l \times K$ frames are encoded in total, of which $m \times (K-1)$ are redundantly processed due to overlap. The effective bitrate R_f is given by

$$R_f = R \cdot \frac{l \times K}{l + (K-1)(l-m)}, \quad (18)$$

where R denotes the original bitrate. In practice, since $m \ll l$, the overhead is negligible. For $l = 48$, $m = 4$, and $K = 2$, the bitrate increases by less than 4.4% while notably improving temporal smoothness across GOP boundaries.

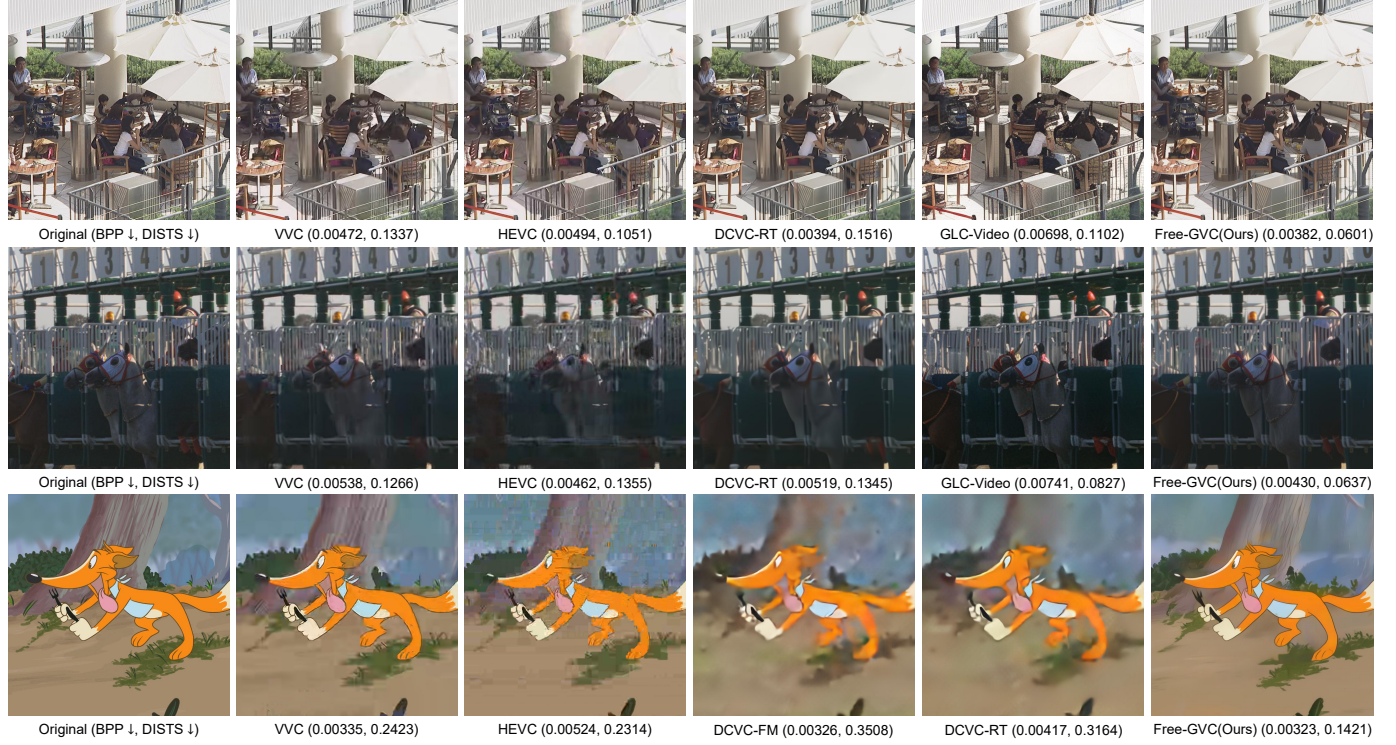


Fig. 7. Visual comparison of reconstructions by different methods. From top to bottom: BQTerrace from HEVC Class B dataset, ReadySteadyGo from UVG dataset, and videoSRC20 from MCL-JCV dataset. Zoom in for better comparison.

It is worth noting that our coding process remains strictly GOP-wise in terms of RCC sampling and entropy coding, with no cross-GOP dependency introduced in the bitstream. And the proposed Inter-GOP Alignment operates only at the reconstruction stage by fusing overlapping latent representations, improving temporal coherence without altering the original encoding-decoding paradigm or compromising GOP-level independence and parallel processing.

V. EXPERIMENTS

A. Experimental Settings

Evaluation Datasets. We evaluate our framework on several widely used video compression benchmarks, including HEVC Class B~E [54], UVG [55], and MCL-JCV [56].

Comparison Methods. We compare our method with three baseline categories, including traditional codecs HEVC [2] and VVC [3], neural codecs DCVC-FM [4] and DCVC-RT [5], and generative codecs DiffC [18] and GLC-Video [16].

Evaluation Metrics. Following [4], [6], [16], [30], we evaluate the first 96 frames of each video sequence. Bit per pixel (BPP) is used to quantify the average number of bits required to encode a single pixel. To assess perceptual quality, we report LPIPS [34] (with AlexNet features by default), DISTs [57], and FID [58]. Following [17], [59], FID is computed on 256×256 image patches. For the HEVC Class D dataset, whose resolution (416×240) is relatively low, we instead compute FID using 64×64 patches as in [60]. Reconstruction fidelity is evaluated using MS-SSIM [61], providing a distortion-oriented reference for more comprehensive

comparison. Temporal consistency is evaluated using tOF and tLP [62], [63], where tOF is based on DIS estimator [64] and tLP measures temporal perceptual variation via LPIPS. We also report BD-Rate and BD-Metric [65] for overall performance comparison, where higher BD-Metric indicates better MS-SSIM and lower values are preferred for perceptual metrics. Negative BD-Rate values denote bitrate savings.

User Study. To comprehensively assess perceptual quality, we conduct a user study following [8], [66] at an ultra-low bitrate of approximately 0.002 bpp. We compare Free-GVC against VVC [3], DCVC-RT [5], and DCVC-RT at double bitrate. An interactive web platform is developed where participants view the reference video alongside two randomly positioned comparison videos that play synchronously. All reconstructed frames are exported as PNG and re-encoded into visually lossless H.265 [2] videos using $\text{crf} = 10$ at 20 fps for fair comparison. Eight sequences are randomly selected from HEVC B~E, UVG, and MCL-JCV datasets, resulting in 24 test groups. Over 20 participants aged 20–40 indicate their preference based on perceptual quality, temporal continuity, and fidelity to the reference. The aggregated preferences provide comprehensive evaluation alongside objective metrics.

Implementation Details. We adopt CogVideoX-2B [52] as the generative prior, which natively supports 480p generation. The VAE encoder and decoder are inherited from CogVideoX-2B, with a temporal downsampling factor $s = 4$, a spatial downsampling factor $d = 8$, and a latent channel dimension of $C = 16$. For high-resolution inputs, we employ a tiling strategy [17], [67], where each frame is partitioned into overlapping 480p tiles and processed independently by the VAE

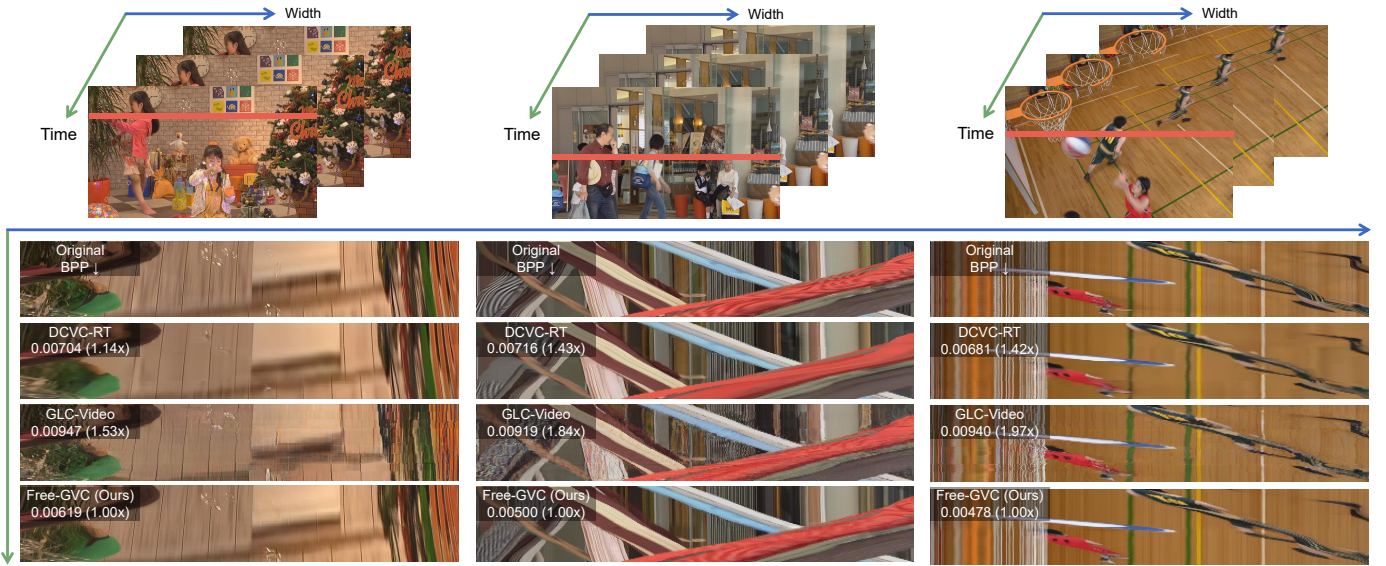


Fig. 8. Visual comparison of temporal coherence by stacking the red line across consecutive frames. Results that are closer to the original indicate better temporal coherence and visual quality. From left to right, the sequences are PartyScene, BQMall, and BasketballDrill from HEVC Class C dataset. Zoom in for better view.

TABLE II. Ablation study on key configurations. The default settings are overlap frames $m = 4$, fusion weight $\gamma(i) = 0.5$, and GOP size $l = 48$. Variants with alternative settings are evaluated, with the best results highlighted in **red**.

Metric	Indicator	Overlap Frames m		Fusion Weight $\gamma(i)$			GOP Size l		Ours
		0	8	0.4	0.6	0.7	32	56	
LPIPS \downarrow	BD-Rate /	8.68 / 0.0031	33.91 / 0.0107	7.43 / 0.0021	3.25 / 0.0010	8.14 / 0.0027	36.39 / 0.0139	6.75 / 0.0024	0.00 / 0.0000
DISTS \downarrow	BD-Metric	-0.93 / -0.0005	44.39 / 0.0091	-6.04 / -0.0015	4.32 / 0.0007	1.83 / 0.0002	39.75 / 0.0091	6.87 / 0.0014	0.00 / 0.0000
tLP \downarrow	Value	0.0254	0.0214	0.0201	0.0201	0.0201	0.0210	0.0204	0.0199
tOF \downarrow	@0.05 BPP	0.3960	0.3654	0.3076	0.3108	0.3070	0.3429	0.3117	0.3061

encoder and diffusion model. The resulting noisy latent tiles are aggregated using a Gaussian weighting map and jointly encoded via RCC to reduce spatial and temporal redundancy. At the decoder, noisy latents are partitioned, denoised, decoded by the VAE, and seamlessly stitched to reconstruct full-resolution frames. By default, videos are divided into GOPs of length $l = 48$ with an overlap of $m = 4$ frames. For inter-GOP alignment, we use a fixed weight $\gamma(i) = 0.5$. Entropy coding is implemented with arithmetic coding.

B. Performance Comparison

Quantitative Results. Fig. 6 and Table I summarize the rate-quality performance on HEVC Class B, C and D, UVG, and MCL-JCV datasets under four evaluation metrics. Overall, our method achieves the best perceptual performance across datasets. In particular, Free-GVC consistently outperforms all competing methods on DISTS and FID, demonstrating superior perceptual quality in terms of structural fidelity and distributional realism. For the distortion-oriented metric MS-SSIM, our method achieves performance comparable to the latest distortion-oriented codecs, while substantially outperforming perception-oriented approaches, indicating that Free-GVC preserves reconstruction fidelity despite operating in the generative compression regime.

We also observe that on 1080p sequences, Free-GVC is slightly inferior to GLC-Video [16] in terms of LPIPS. A possible explanation is that the video diffusion prior is trained on relatively low-resolution data. While tiling effectively enables high-resolution inference and preserves global structure, the model may still face challenges in consistently modeling fine-grained perceptual details across tiles at large resolutions, which can impact LPIPS. This trend is consistent with the results on the HEVC C and D datasets, where our method shows more pronounced advantages on lower-resolution videos. Moreover, LPIPS has inherent limitations as a perceptual metric, particularly at ultra-low bitrates, as it emphasizes pixel-level feature differences rather than semantic consistency or texture realism [16], [17], [57]. We therefore primarily rely on DISTS for perceptual comparison, as it better correlates with human perception in compression scenarios.

Qualitative Results. Fig. 7 presents a visual comparison of decoded frames from different methods. At ultra-low bitrates, distortion-oriented codecs such as HEVC [2], VVC [3], DCVC-FM [4], and DCVC-RT [5] exhibit noticeable blocking artifacts and motion ghosting. Perception-oriented generative methods like GLC-Video [16] improve visual realism but may introduce spatial inconsistencies, producing visually plausible yet content-inaccurate details. In contrast, our approach leverages the video diffusion prior to jointly model spa-

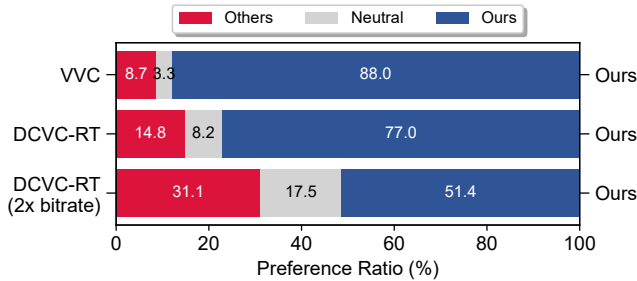


Fig. 9. User study on randomly selected videos shows that our method surpasses VVC and DCVC-RT at the same bitrates and even outperforms DCVC-RT at half its bitrate.

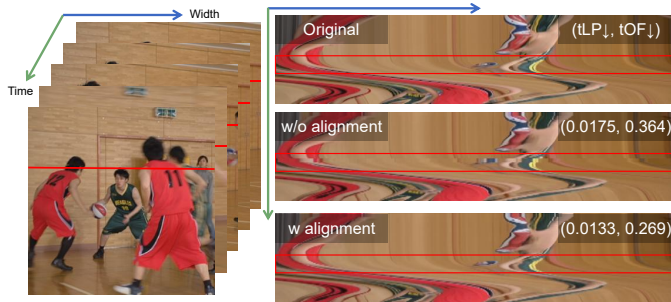


Fig. 10. Comparison of temporal consistency with and without the Inter-GOP Alignment mechanism, visualized by stacking the red line over time. Zoom in for a clearer comparison.

tial and temporal redundancies, achieving ultra-low bitrate compression while preserving both perceptual fidelity and temporal coherence. Additional qualitative results and video demonstrations are provided in the supplementary material.

Fig. 8 further highlights temporal coherence. In regions with cross-frame object motion, DCVC-RT [5] produces heavy blur, while GLC-Video [16] exhibits visible flickering on moving elements, leading to unstable visual quality. Free-GVC, by contrast, maintains sharp per-frame details and smooth temporal transitions, accurately reconstructing intricate textures in motion-affected areas without introducing artifacts. These results demonstrate the superior perceptual quality and temporal consistency of our method.

User Study. We conduct a user study on randomly selected video sequences to evaluate perceptual quality, temporal coherence, and fidelity among our method, DCVC-RT [5], and VVC [3]. As shown in Fig. 9, our approach is preferred over both neural and traditional codecs at similar bitrates. In particular, even when operating at roughly half the bitrate of DCVC-RT, our method wins in 51.4% of the comparisons, demonstrating that it can achieve perceptually superior results while significantly reducing bitrate.

C. Ablation Study

We conduct ablation studies on the HEVC Class D dataset, and the main results are summarized in Table II.

Inter-GOP Alignment. Fig. 10 shows the temporal variation of pixel values at the same location before and after applying our alignment strategy. Without alignment, frames

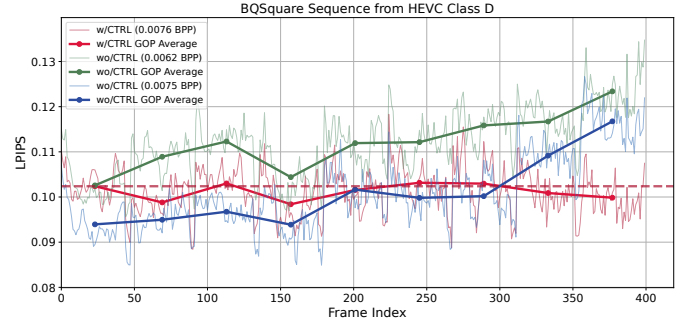


Fig. 11. LPIPS variation across frame indexes, comparing results with and without the proposed quality control algorithm.

TABLE III. Detailed runtime of various modules on HEVC C dataset at 480p using NVIDIA GTX 4090.

Timestep	MS-SSIM \uparrow	DISTS \downarrow	VAE Enc.	Diffusion	RCC	Enc. FPS
50	0.9594	0.0711	0.0555	0.522	3.349	0.254
100	0.9503	0.0764	0.0555	0.436	2.598	0.323
200	0.9280	0.0966	0.0555	0.293	1.564	0.522
300	0.9047	0.0986	0.0555	0.221	1.118	0.716
400	0.8738	0.112	0.0555	0.172	0.844	0.932
500	0.8230	0.133	0.0555	0.123	0.543	1.38

(a) Encoding time (seconds) and FPS

Timestep	BPP \downarrow	Diffusion	RCC	Denoise	VAE Dec.	Dec. FPS
50	0.0152	0.507	2.48	0.0228	0.111	0.319
100	0.0099	0.422	1.968	0.0318	0.113	0.394
200	0.0047	0.278	1.24	0.0591	0.109	0.589
300	0.0028	0.206	0.912	0.0773	0.111	0.764
400	0.0018	0.157	0.678	0.100	0.112	0.954
500	0.0011	0.107	0.459	0.123	0.109	1.250

(b) Decoding time (seconds) and FPS

remain smooth within each GOP but exhibit artifacts at GOP boundaries. Inter-GOP alignment effectively reduces these inconsistencies, producing variations that closely follow the ground truth. We further examine the impact of the number of overlapping frames m between adjacent GOPs. A small overlap with $m = 4$ slightly increases bitrate but improves temporal continuity and perceptual quality, often yielding comparable or better BD-Rate results, whereas enlarging the overlap to $m = 8$ introduces redundant overhead and may amplify inconsistencies. Experiments on the fusion weight $\gamma(i)$ indicate that 0.5 balances temporal smoothness and fidelity.

GOP Size. We study the impact of different GOP lengths and find that a size l of 48 achieves the best overall performance. This choice aligns well with the default sequence length of the pre-trained CogVideoX diffusion model [52], ensuring optimal utilization of temporal information.

Quality Control. Fig. 11 shows the effect of our quality control across GOPs. We evaluate on the first 400 frames of each video. Without this mechanism, content variations cause large fluctuations in reconstruction quality. In contrast, our method uses the quality metric of the first GOP as a target to guide subsequent GOPs, dynamically adjusting the encoding process to maintain stable perceptual quality. With prediction reuse enabled, only two to three decoding iterations

are typically required to obtain an accurate quality estimate, compared to five to seven iterations without reuse.

D. Complexity Analysis

Table III summarizes the encoding and decoding runtime of our pipeline. The encoding phase consists of VAE encoding, diffusion-based distribution estimation, and RCC compression. The decoding phase mirrors these operations with additional steps for unconditional denoising and VAE decoding.

As a progressive coding framework, higher target bitrates correspond to more diffusion and RCC steps, resulting in a near-linear increase in encoding and decoding latency. We observe that RCC runtime scales more rapidly with bitrate than the diffusion computations themselves. Despite this, our method achieves 1.25 frames per second (fps) at 0.001 bpp, significantly outperforming existing diffusion-based codecs like DiffVC [19], which operates at only 0.25 fps across all bitrates. While real-time processing remains challenging, further acceleration is possible through RCC optimization [68], [69] and diffusion speed-up techniques [70]–[72].

VI. CONCLUSION

This paper presents a training-free generative video compression framework, termed Free-GVC, which leverages pre-trained video diffusion models to jointly capture both spatial and temporal dependencies. By reformulating compression as progressive latent coding within the diffusion space, our method achieves perceptually faithful and visually coherent reconstruction at ultra-low bitrates. The Inter-GOP Alignment module effectively mitigates boundary artifacts and enhances temporal consistency, while the Adaptive Quality Control mechanism dynamically stabilizes perceptual quality across diverse content and GOPs.

Despite its strong performance, achieving real-time compression for high-resolution videos remains challenging for this framework. Nevertheless, this limitation can be alleviated through future optimization, highlighting a promising direction for generative video compression.

REFERENCES

- [1] T. Wiegand, G. J. Sullivan, G. Bjontegaard, and A. Luthra, “Overview of the h.264/avc video coding standard,” *IEEE Trans. Circuits Syst. Video Technol.*, vol. 13, no. 7, pp. 560–576, 2003.
- [2] G. J. Sullivan, J. Ohm, W. Han, and T. Wiegand, “Overview of the high efficiency video coding (HEVC) standard,” *IEEE Trans. Circuits Syst. Video Technol.*, vol. 22, no. 12, pp. 1649–1668, 2012.
- [3] B. Bross, Y.-K. Wang, Y. Ye, S. Liu, J. Chen, G. J. Sullivan, and J.-R. Ohm, “Overview of the versatile video coding (vvc) standard and its applications,” *IEEE Trans. Circuits Syst. Video Technol.*, vol. 31, no. 10, pp. 3736–3764, 2021.
- [4] J. Li, B. Li, and Y. Lu, “Neural video compression with feature modulation,” in *Proc. IEEE/CVF Conf. Comput. Vis. Pattern Recognit.* IEEE, 2024, pp. 26 099–26 108.
- [5] Z. Jia, B. Li, J. Li, W. Xie, L. Qi, H. Li, and Y. Lu, “Towards practical real-time neural video compression,” in *Proc. IEEE/CVF Conf. Comput. Vis. Pattern Recognit.*, 2025, pp. 12 543–12 552.
- [6] W. Jiang, J. Li, K. Zhang, and L. Zhang, “Ecvc: Exploiting non-local correlations in multiple frames for contextual video compression,” in *Proc. IEEE/CVF Conf. Comput. Vis. Pattern Recognit.*, 2025, pp. 7331–7341.
- [7] M. Li, Y. Shi, J. Wang, and Y. Huang, “High visual-fidelity learned video compression,” in *Proc. ACM Int. Conf. Multimedia*, 2023, pp. 8057–8066.
- [8] F. Mentzer, E. Agustsson, J. Ballé, D. Minnen, N. Johnston, and G. Toderici, “Neural video compression using gans for detail synthesis and propagation,” in *Proc. Eur. Conf. Comput. Vis.* Springer, 2022, pp. 562–578.
- [9] R. Yang, R. Timofte, and L. V. Gool, “Perceptual learned video compression with recurrent conditional GAN,” in *Proc. Int. Joint Conf. Artif. Intell.*, 2022, pp. 1537–1544.
- [10] D. Podell, Z. English, K. Lacey, A. Blattmann, T. Dockhorn, J. Müller, J. Penna, and R. Rombach, “SDXL: improving latent diffusion models for high-resolution image synthesis,” in *Int. Conf. Learn. Represent.*, 2024.
- [11] T. Brooks, B. Peebles, C. Holmes, W. DePue, Y. Guo, L. Jing, D. Schnurr, J. Taylor, T. Luhman, E. Luhman, C. Ng, R. Wang, and A. Ramesh, “Video generation models as world simulators,” 2024. [Online]. Available: <https://openai.com/research/video-generation-models-as-world-simulators>
- [12] B. F. Labs, “Flux.1 kontext: Flow matching for in-context image generation and editing in latent space,” *arXiv preprint arXiv:2506.15742*, 2025.
- [13] Z. Li, Y. Zhou, H. Wei, C. Ge, and J. Jiang, “Toward extreme image compression with latent feature guidance and diffusion prior,” *IEEE Trans. Circuits Syst. Video Technol.*, vol. 35, no. 1, pp. 888–899, 2025.
- [14] M. Careil, M. J. Muckley, J. Verbeek, and S. Lathuilière, “Towards image compression with perfect realism at ultra-low bitrates,” in *Int. Conf. Learn. Represent.*, 2023.
- [15] L. Theis, T. Salimans, M. D. Hoffman, and F. Mentzer, “Lossy compression with gaussian diffusion,” *arXiv preprint arXiv:2206.08889*, 2022.
- [16] L. Qi, Z. Jia, J. Li, B. Li, H. Li, and Y. Lu, “Generative latent coding for ultra-low bitrate image and video compression,” *IEEE Trans. Circuits Syst. Video Technol.*, 2025.
- [17] T. Zhang, X. Luo, L. Li, and D. Liu, “Stablecodec: Taming one-step diffusion for extreme image compression,” in *Proc. IEEE/CVF Int. Conf. Comput. Vis.*, 2025.
- [18] J. Vonderfecht and F. Liu, “Lossy compression with pretrained diffusion models,” in *Int. Conf. Learn. Represent.*, 2025.
- [19] W. Ma and Z. Chen, “Diffusion-based perceptual neural video compression with temporal diffusion information reuse,” *ACM Trans. Multimedia Comput. Commun. Appl.*, vol. 21, no. 12, pp. 1–22, 2025.
- [20] B. Li, Y. Liu, X. Niu, B. Bait, W. Han, L. Deng, and D. Gunduz, “Extreme video compression with prediction using pre-trained diffusion models,” in *Proc. Int. Conf. Wireless Commun. Signal Process.* IEEE, 2024, pp. 1449–1455.
- [21] Z. Wang, H. Man, W. Li, X. Wang, X. Fan, and D. Zhao, “T-gvc: Trajectory-guided generative video coding at ultra-low bitrates,” *arXiv preprint arXiv:2507.07633*, 2025.
- [22] Y.-H. Chen, Y.-C. Yao, K.-W. Ho, C.-H. Wu, H.-T. Phung, M. Benjak, J. Ostermann, and W.-H. Peng, “Hytip: Hybrid temporal information propagation for masked conditional residual video coding,” in *Proc. IEEE/CVF Int. Conf. Comput. Vis.*, 2025.
- [23] J. Liao, Y. Wu, C. Lin, Z. Deng, L. Li, D. Liu, and X. Sun, “Ehvc: Efficient hierarchical reference and quality structure for neural video coding,” in *Proc. ACM Int. Conf. Multimedia*, 2025.
- [24] X. Sheng, L. Li, D. Liu, and H. Li, “Prediction and reference quality adaptation for learned video compression,” *IEEE Trans. Image Process.*, 2025.
- [25] Y. Bian, C. Tang, L. Li, and D. Liu, “Augmented deep contexts for spatially embedded video coding,” in *Proc. IEEE/CVF Conf. Comput. Vis. Pattern Recognit.*, 2025, pp. 2094–2104.
- [26] C. Tang, Z. Li, Y. Bian, L. Li, and D. Liu, “Neural video compression with context modulation,” in *Proc. IEEE/CVF Conf. Comput. Vis. Pattern Recognit.*, 2025, pp. 12 553–12 563.
- [27] G. Gao, S. Teng, T. Peng, F. Zhang, and D. Bull, “Givic: Generative implicit video compression,” in *Proc. IEEE/CVF Int. Conf. Comput. Vis.*, 2025, pp. 17 356–17 367.
- [28] G. Lu, W. Ouyang, D. Xu, X. Zhang, C. Cai, and Z. Gao, “DVC: an end-to-end deep video compression framework,” in *Proc. IEEE/CVF Conf. Comput. Vis. Pattern Recognit.*, 2019, pp. 11 006–11 015.
- [29] J. Li, B. Li, and Y. Lu, “Deep contextual video compression,” in *Adv. Neural Inf. Process. Syst.*, 2021, pp. 18 114–18 125.
- [30] ———, “Neural video compression with diverse contexts,” in *Proc. IEEE/CVF Conf. Comput. Vis. Pattern Recognit.*, 2023, pp. 22 616–22 626.
- [31] M. Lu, Z. Duan, F. Zhu, and Z. Ma, “Deep hierarchical video compression,” in *Proc. AAAI Conf. Artif. Intell.*, vol. 38, no. 8, 2024, pp. 8859–8867.

[32] M. Lu, Z. Duan, W. Cong, D. Ding, F. Zhu, and Z. Ma, "High-efficiency neural video compression via hierarchical predictive learning," *arXiv preprint arXiv:2410.02598*, 2024.

[33] S. Zhang, M. Mrak, L. Herranz, M. G. Blanch, S. Wan, and F. Yang, "Dvc-p: Deep video compression with perceptual optimizations," in *Proc. IEEE Vis. Commun. Image Process.* IEEE, 2021, pp. 1–5.

[34] R. Zhang, P. Isola, A. A. Efros, E. Shechtman, and O. Wang, "The unreasonable effectiveness of deep features as a perceptual metric," in *Proc. IEEE/CVF Conf. Comput. Vis. Pattern Recognit.*, 2018, pp. 586–595.

[35] I. Goodfellow, J. Pouget-Abadie, M. Mirza, B. Xu, D. Warde-Farley, S. Ozair, A. Courville, and Y. Bengio, "Generative adversarial nets," *Adv. Neural Inf. Process. Syst.*, vol. 27, 2014.

[36] P. Esser, R. Rombach, and B. Ommer, "Taming transformers for high-resolution image synthesis," in *Proc. IEEE/CVF Conf. Comput. Vis. Pattern Recognit.*, 2021, pp. 12873–12883.

[37] W. Ma and Z. Chen, "Diffvc-osd: One-step diffusion-based perceptual neural video compression framework," *arXiv preprint arXiv:2508.07682*, 2025.

[38] Y. Mao, M. Wang, S. Wang, and S. Kwong, "High efficiency rate control for versatile video coding based on composite cauchy distribution," *IEEE Trans. Circuits Syst. Video Technol.*, vol. 32, no. 4, pp. 2371–2384, 2021.

[39] L. Feng, Q. Yin, and S. Ma, "Content-adaptive rate control method for user-generated content videos," *IEEE Trans. Circuits Syst. Video Technol.*, 2024.

[40] J. Liao, L. Li, D. Liu, and H. Li, "Content-adaptive rate-distortion modeling for frame-level rate control in versatile video coding," *IEEE Trans. Multimedia*, vol. 26, pp. 6864–6879, 2024.

[41] Y. Li, X. Chen, J. Li, J. Wen, Y. Han, S. Liu, and X. Xu, "Rate control for learned video compression," in *Proc. IEEE Int. Conf. Acoust. Speech Signal Process.* IEEE, 2022, pp. 2829–2833.

[42] C. Zhang and W. Gao, "Learned rate control for frame-level adaptive neural video compression via dynamic neural network," in *Proc. Eur. Conf. Comput. Vis.* Springer, 2024, pp. 239–255.

[43] J. Chen, M. Wang, P. Zhang, S. Wang, and S. Wang, "Sparse-to-dense: High efficiency rate control for end-to-end scale-adaptive video coding," *IEEE Trans. Circuits Syst. Video Technol.*, vol. 34, no. 5, pp. 4027–4039, 2023.

[44] Y. Zhang, G. Lu, Y. Chen, S. Wang, Y. Shi, J. Wang, and L. Song, "Neural rate control for learned video compression," in *Int. Conf. Learn. Represent.*, 2024.

[45] B. Gu, H. Chen, M. Lu, J. Yao, and Z. Ma, "Adaptive rate control for deep video compression with rate-distortion prediction," in *Proc. Data Compression Conf.* IEEE, 2025, pp. 33–42.

[46] L. Feng, Q. Yin, J. Zhang, Y. He, and S. Ma, "High accuracy rate control for neural video coding based on rate-distortion modeling," *IEEE Trans. Circuits Syst. Video Technol.*, 2025.

[47] J. Ho, A. Jain, and P. Abbeel, "Denoising diffusion probabilistic models," in *Adv. Neural Inf. Process. Syst.*, 2020.

[48] P. Harsha, R. Jain, D. McAllester, and J. Radhakrishnan, "The communication complexity of correlation," in *Proc. IEEE Conf. Comput. Complexity*. IEEE, 2007, pp. 10–23.

[49] M. Havasi, R. Pecharz, and J. M. Hernández-Lobato, "Minimal random code learning: Getting bits back from compressed model parameters," in *Int. Conf. Learn. Represent.*, 2019.

[50] L. Theis and N. Y. Ahmed, "Algorithms for the communication of samples," in *Int. Conf. Mach. Learn.*, vol. 162, 2022, pp. 21308–21328.

[51] C. T. Li and A. El Gamal, "Strong functional representation lemma and applications to coding theorems," *IEEE Trans. Inf. Theory*, vol. 64, no. 11, pp. 6967–6978, 2018.

[52] Z. Yang, J. Teng, W. Zheng, and et al., "Cogvideox: Text-to-video diffusion models with an expert transformer," in *Int. Conf. Learn. Represent.*, 2025.

[53] T. Wan, "Wan: Open and advanced large-scale video generative models," *arXiv preprint arXiv:2503.20314*, 2020.

[54] D. Flynn, K. Sharman, and C. Rosewarne, "Common Test Conditions and Software Reference Configurations for HEVC Range Extensions, document JCTVC-N1006," *Joint Collaborative Team Video Coding ITU-T SG*, vol. 16, 2011.

[55] A. Mercat, M. Vitanen, and J. Vanne, "UVG dataset: 50/120fps 4K sequences for video codec analysis and development," in *Proc. ACM Multimedia Syst. Conf.*, 2020, pp. 297–302.

[56] H. Wang, W. Gan, S. Hu, J. Y. Lin, L. Jin, L. Song, P. Wang, I. Katsavounidis, A. Aaron, and C.-C. J. Kuo, "MCL-JCV: a JND-based H. 264/AVC video quality assessment dataset," in *Proc. IEEE Int. Conf. Image Process.* IEEE, 2016, pp. 1509–1513.

[57] K. Ding, K. Ma, S. Wang, and E. P. Simoncelli, "Image quality assessment: Unifying structure and texture similarity," *IEEE Trans. Pattern Anal. Mach. Intell.*, vol. 44, no. 5, pp. 2567–2581, 2022.

[58] M. Heusel, H. Ramsauer, T. Unterthiner, B. Nessler, and S. Hochreiter, "Gans trained by a two time-scale update rule converge to a local nash equilibrium," in *Adv. Neural Inf. Process. Syst.*, 2017, pp. 6626–6637.

[59] Z. Jia, J. Li, B. Li, H. Li, and Y. Lu, "Generative latent coding for ultra-low bitrate image compression," in *Proc. IEEE/CVF Conf. Comput. Vis. Pattern Recognit.*, 2024, pp. 26088–26098.

[60] Z. Jia, Z. Zheng, N. Xue, J. Li, B. Li, Z. Guo, X. Zhang, H. Li, and Y. Lu, "Cod: A diffusion foundation model for image compression," *arXiv preprint arXiv:2511.18706*, 2025.

[61] Z. Wang, E. P. Simoncelli, and A. C. Bovik, "Multiscale structural similarity for image quality assessment," in *Proc. Asilomar Conf. Signals Syst. Comput.* IEEE, 2003.

[62] J. Oh and M. Kim, "Demfi: Deep joint deblurring and multi-frame interpolation with flow-guided attentive correlation and recursive boosting," in *Proc. Eur. Conf. Comput. Vis.*, 2022.

[63] G. Youk, J. Oh, and M. Kim, "Fma-net: Flow-guided dynamic filtering and iterative feature refinement with multi-attention for joint video super-resolution and deblurring," in *Proc. IEEE/CVF Conf. Comput. Vis. Pattern Recognit.*, June 2024, pp. 44–55.

[64] T. Kroeger, R. Timofte, D. Dai, and L. V. Gool, "Fast optical flow using dense inverse search," in *Proc. Eur. Conf. Comput. Vis.*, 2016.

[65] G. Bjontegaard, "Calculation of average psnr differences between rd-curves," *ITU-T SG16, Doc. VCEG-M33*, 2001.

[66] F. Mentzer, G. Toderici, M. Tschanne, and E. Agustsson, "High-fidelity generative image compression," in *Adv. Neural Inf. Process. Syst.*, 2020.

[67] J. Wang, Z. Yue, S. Zhou, K. C. K. Chan, and C. C. Loy, "Exploiting diffusion prior for real-world image super-resolution," *Int. J. Comput. Vis.*, vol. 132, no. 12, pp. 5929–5949, 2024.

[68] G. Ohayon, H. Manor, T. Michaeli, and M. Elad, "Compressed image generation with denoising diffusion codebook models," in *Int. Conf. Mach. Learn.*, 2025.

[69] A. Vaisman, G. Ohayon, H. Manor, M. Elad, and T. Michaeli, "Turbo-DDCM: Fast and flexible zero-shot diffusion-based image compression," *arXiv preprint:2511.06424*, 2025.

[70] X. Ma, G. Fang, and X. Wang, "Deepcache: Accelerating diffusion models for free," in *Proc. IEEE/CVF Conf. Comput. Vis. Pattern Recognit.*, 2024.

[71] G. Fang, X. Ma, and X. Wang, "Structural pruning for diffusion models," in *Adv. Neural Inf. Process. Syst.*, 2023.

[72] G. Fang, K. Li, X. Ma, and X. Wang, "Tinyfusion: Diffusion transformers learned shallow," in *Proc. IEEE/CVF Conf. Comput. Vis. Pattern Recognit.*, 2025, pp. 18144–18154.